INTERNATIONAL JOURNAL OF ADVANCED ENGINEERING AND BUSINESS SCIENCES (IJAEBS)

Journal homepage: https://ijaebs.journals.ekb.eg

Simulating of R.C Frames under Progressive Collapse Using AEM

F.B.A. Beshara[a], O.O. El-Mahdy[b] , Ahmed. A. Mahmoud[*c] and M.A.A. Abbass[d]

[a] Associate Professor, Department of civil engineering, faculty of engineering (Shoubra), Benha University,108 Shoubra St., Shoubra, Cairo, Egypt

[b] Professor of Structures, Department of civil engineering, faculty of engineering (Shoubra), Benha University,108 Shoubra St., Shoubra, Cairo, Egypt

[c] Professor of Reinforced Concrete Structures, Department of civil engineering, faculty of engineering (Shoubra), Benha University,108 Shoubra St., Shoubra, Cairo, Egypt

[d] Assistance Lecture, Department of civil engineering, faculty of engineering (Shoubra), Benha University,108 Shoubra St., Shoubra, Cairo, Egypt

*Corresponding author: Email address: ahmed.m5882@gmail.com

Received: 24-09-2022 **Accepted:** 13-11-2022 **Published**: 01-02-2023

ABSTRACT

The purpose of the present research is to review the Applied Element Method (AEM) formulation and its implementation in the commercial software Extreme Loading for Structures (ELS) to study the progressive collapse of R.C frames. Also, the properties and capacities of (ELS) used to simulate and describe the progressive collapse events. This paper focuses on the progressive collapse of 2-D and 3-D reinforced concrete frames, provides a validation for (AEM) using (ELS) by simulating and modeling four reinforced concrete frames tested experimentally in laboratories by other researchers. To verify (ELS), the frames are modeled numerically using (ELS) with the same loading technique, concrete dimensions and reinforcement details of the tested frames, then the results are compared with the experimental results to validate AEM. A 2-D three-story frame is modeled with interior column removal study. The second validated frame was a 2-D two-story frame with interior column removal. The third validated specimen was a 3-D single-story frame with corner column removal. Also a 3-D three-story frame is modeled with central edge column removal. The 3-D frames are studied taken into consideration the contribution of slabs to determine the effect of different structural elements in progressive collapse. Crack pattern, deformed shape, load deformation curve, concrete strains and steel

strains are obtained from numerical models and are compared with the experimental results. Generally, the numerical results are in a good agreement with experimental ones.

Keywords: Reinforced concrete frames; Progressive collapse; Simulation; Validation; Load displacement curves; Steel strain curves; Crack patterns; Applied element method (AEM); Extreme Loading for Structures (ELS).

1 INTRODUCTION

Several structural progressive collapses accidentally took place in the last few decades [1]. For example, in 1968, the collapse of the 22-story Ronan building [2], East London took place due to gas explosion in 18th floor. In 1995, the Murrah Federal Office Building in Oklahoma City was collapsed after a terrorist bomb explosion at the ground floor [3]. In 2001, the World Trade Center [4], New York, was totally demolished due to planes impact at the tower upper levels. Recently, design guidelines such as General Services Administration (GSA) [5] and the Unified Facilities Criteria (UFC) [6] addressed progressive collapse due to sudden loss of a main vertical support. Many thoughtful kinds of reviews have been conducted to discuss the current advanced results and future developments on experimental studies and theoretical analysis, on the progressive collapse resistance of frame structures [7]. Zhang and Zhao et al. [8] and [9] developed a simplified model for considering the contribution of floor slab on progressive collapse resistance of frames. The (AEM) was settled in 1995 as part of research studies, developed by [10]. However, only in 2000 the term of "Applied Element Method" was presented in a research paper [11]. Then, the mechanism of this solving method was applied for each case of analysis such as, elastic analysis [11], crack initiation, propagation and estimation of failure loads of reinforced concrete structures [11]. The nonlinear numerical techniques conventionally used in structural analysis can be divided into two groups. For the first group, the model is depending on continuum material equations. The most common example for the first group is the finite element method (FEM). (FEM) is expressed with dividing the province into finite elements with the respective material properties. Good results of (FEM) as a structural analysis before collapse are provided by considering geometry and materials nonlinearity. By changing the structure behavior to progressive collapse, results of crack propagation and opening are required. The (FEM) loses its efficiency under this structure behavior.

The second group can be represented by the discrete element techniques. For this technique, the mechanical connection between elements is allowed and the cracking simulation processing becomes more simply when comparing with FEM. However, the advantages of FEM compared to Discrete

Element Methods (DEM) is that it is more accurate in the small displacement analysis. In order to overcome the DEM's problems, Tagel-Din and Meguro [10] created the Applied Element Method [11]. ELS also can be used in nonlinear dynamic analysis for low rise and high rise reinforced concrete buildings [12]. The main advantage of the AEM is its capability to represent the structure's behavior from zero loading till collapse, through the elastic phase, opening and propagation of cracks, yielding of mail reinforcement steel and separation and collision of elements, as shown in Figure (1). However, the computation time required to simulate large structure's behavior from zero loading till collapse might become very large due to the necessity of small-time increments, in order to ensure numerical stability.

2 GEOMETRICAL MODELING OF THE STRUCTURAL ELEMENTS

2.1 Elements Generated in AEM

In the AEM, the structure is modelled as a group of small rigid prisms, as indicated in Figure (2). Connections between the adjacent prisms are couples of normal and shear nonlinear springs (one normal and two shear springs) spread along the element interface and located at the contacted points. These springs represent the stresses, strains and deformations of each element. The AEM is a stiffness-based method, in which the stiffness of each pair of normal (K_n) and shear (K_s) springs connecting the element centerlines is calculated as in equations (1) and (2).

$$K_n = \left(\frac{\mathrm{E} \times \mathrm{d} \times \mathrm{t}}{a}\right) \quad (1)$$

$$K_s = \left(\frac{\mathrm{G} \times \mathrm{d} \times \mathrm{t}}{a}\right) \quad (2)$$

Where (d) is the distance between springs, (t) is the thickness of the element and (a) is the length of the representative area, E and G are the young's and shear modulus of the material, respectively. As observed in Figure (2), stresses and deformations of a certain volume for 3-D analysis or a certain area for 2-D analysis are defined by package of springs. At the location of the reinforcement bar, the reinforcement bar replaces this area. In 2-D element formulation, there are three degrees of freedom (DOF) used to represent the rigid body motion of each element. Although the element's motion is a rigid body motion. The group of elements is deformable, and thus, its internal stresses and deformations are calculated by its springs. The total stiffness matrix of each element can be given by the summation of the stiffness matrices of individual couples of springs. The contact springs depend

upon the axial and shear stiffness as well as the location. So, the average stiffness matrix for the element gives the resultant over all stiffness, according to the stress situation around it. Referring to [11], it is possible to define the governing equation as:

$$[K_G]\,\{u\} = \{F\} \qquad (3)$$

Where $[K_G]$ is the global stiffness matrix, {u} is the displacement vector and {F} the applied load vector. The AEM allows for both displacement and load control. At start, the applied load vector {f} is known before performing the analysis. Then, the load vector becomes unknown and should be determined by applying a unit displacement to one or more degrees of freedom. Also, one should consider the element rotation. The theoretical rotational stiffness K_r can be calculated from normal springs as [11]:

$$K_r = \int_{-b/2}^{b/2} \frac{Et}{b} Z^2 \quad = \frac{Etb^2}{12} \qquad (4)$$

Where t is the thickness of the element, b the element's height, E is the young's modulus, and z the spring's distance to the element centroid as represented in Figure (3).

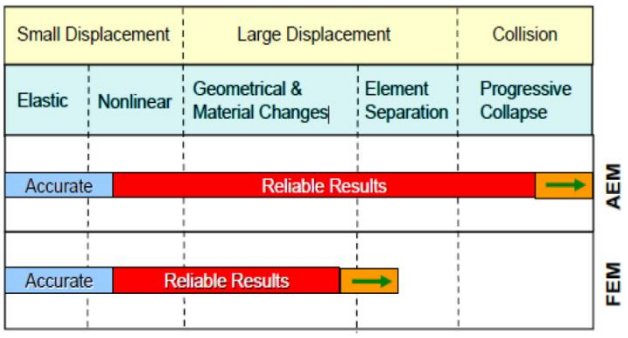

Figure (1) Analysis Domain of AEM Compared to FEM [1].

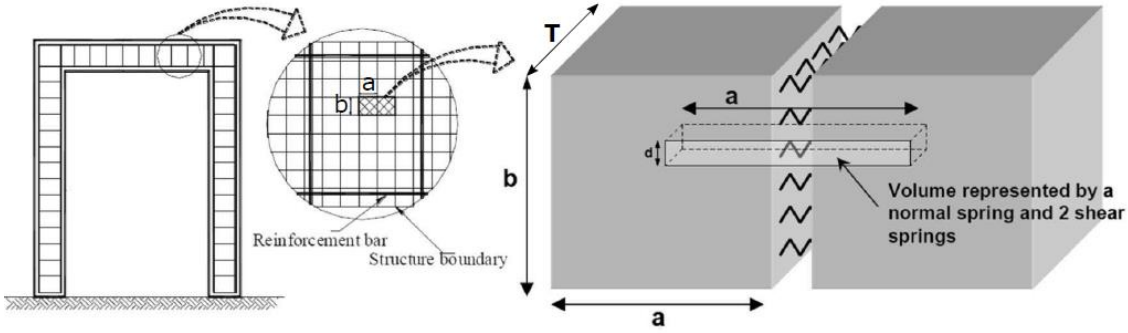

Figure (2) Modelling of Structure using AEM [11].

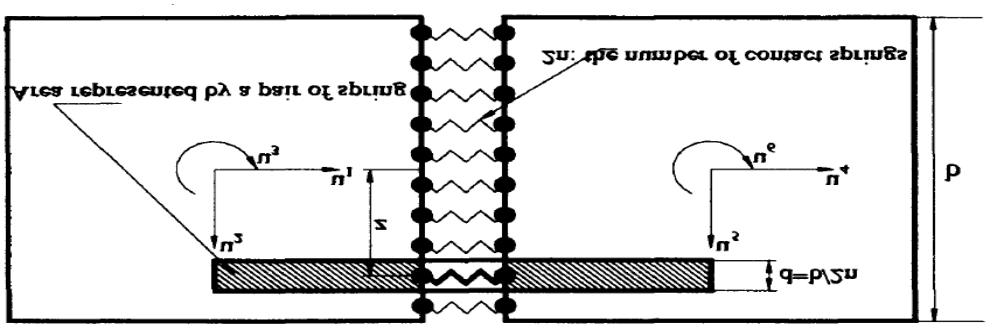

Figure (3) Normal Springs for Rotational Stiffness [11].

2.2 Geometry Issues for R.C Models in (ELS) Software

To model a 2-D reinforced concrete frame in (ELS) it is not necessary to unify meshing between girders and columns (Mesh-Free methods), as parts should not be connected together through nodes as in finite element method (FEM) [13]. Contrary to FEM, the same two elements are connected automatically with AEM. This property is one of causes why AEM is much faster in modeling. Since reinforcement bars are modeled using springs, it is normal for the program to determine the start, the end, area and material of all reinforcement bars in the model to produce all steel springs. To model slab in 3-D R.C model, slabs reinforcement should intersect with adjacent beams to make slab very stiff, and meshing of slab at fallen part should be increased more than other slabs connected to non-fallen parts.

To generate a moment connection between girder and column in (ELS), steel rebars of girder should intersect with the column or extend to columns cross section. If the rebars does not extend to columns cross section, the connection between girder and column would represent a hinged connection (no moment will transfer between column and girders). Figures (4) and (5), show the analysis results of two frames; each consisted of one bay and have the same concrete dimensions and the same reinforcement [13]. The first one of them has a bar extension length equals zero, while the other has a positive and negative extension lengths.

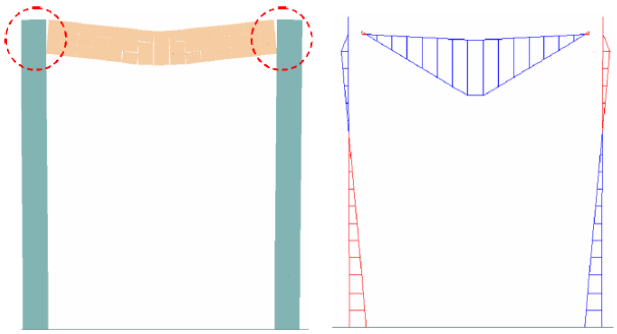

Figure (4) Case 1: Reinforcement of Beam is not Extended in the Column (Hinged Connection).

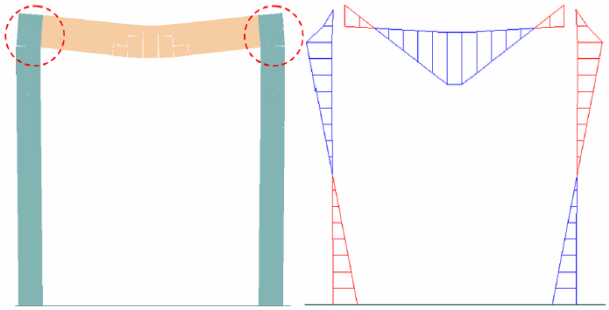

Figure (5) Case 2: Reinforcement of Beam is Extended in the Column (Rigid Connection).

3 MATERIAL MODELLING

3.1 Concrete Model

For concrete in compression, Figure (6) presents the constitutive models involved in ELS for concrete in compression. To model concrete under compression, Okamura and Maekawa model [14] is adopted. In this model, concrete is described as a combination of elements parallel to each other. Each element consists of an elastic spring and a plastic slider. The plastic parts represent the plasticity related to the degree of accumulated damage and the number of broken elastic springs represents the compressive fracture leading to a reduction of the stiffness and the initial Young's modulus E_0. The fracture parameter K_0, which representing the extent of the internal damage of concrete and the compressive plastic strain are presented to define the envelope for compressive stresses and compressive strains. The envelop stress-strain curve for concrete in compression (elasto-plastic and fracture model) is expressed by the following equations [14]:

$$\sigma_c = K_0 . \mathrm{E}_0 \, (\varepsilon - \varepsilon_P) \tag{7}$$

$$K_0 = e^{-0.73 .\, x\,(1-e^{-1.25x})} \tag{8}$$

$$\mathrm{E}_0 = \frac{2f'_c}{\varepsilon_{peak}} \tag{9}$$

$$\varepsilon_P = \varepsilon_{Peak} \left(x - \frac{20}{7} \left(1 - e^{-0.35\, x}\right)\right) \tag{10}$$

$$x = \frac{\varepsilon}{\varepsilon_{Peak}} \tag{11}$$

Where, K_0 is the fracture parameter represents the damage of concrete, E_0 is the initial stiffness of concrete, ε_P is the plastic strain corresponding to the total strain, ε_{Peak} is the peak strain for concrete under compression, f'_c is the specified concrete compressive strength, ε is the strain in compression and *x* is the ratio between the strain in compression and peak strain.

For concrete springs subjected to tension, when reaching the ultimate strength, the spring's stiffness is supposed as 0.1% of the original value to sustain connection between elements to get out of the negative stiffness values as shown in Figure (6). Concrete stiffness of the tension springs is assumed as constant until the spring reaches the cracking point. After this point, stiffness is regarded as zero and the residual stresses are redistributed. The envelop stress-strain curve for concrete in tension is expressed by the following equations [14]:

$$\sigma_t = f_t\left(\frac{\varepsilon_{cr}}{\varepsilon}\right)^{0.4} \quad (12)$$

Where, f_t is the tensile concrete strength, ε_{cr} is the cracking strain and ε is the strain in tension.

Figure (7) describes the model of concrete performance in shear [15]. It is considered as a linear till reaches the cracking strain. When the springs reach the cracking principle strain, the whole shear strength value at the face of the crack is redistributed (the Redistribution Value RV=1.0). In order to represent the effects of shear friction and interlocking, a redistributed proportion of the shear stresses, RV, assumed to be 0.5, is considered. The stress-strain relationship for shear is expressed by two straight lines as follows [15]:

$$\tau_{cr} = 3.8\,(f'_c)^{(\frac{1}{3})}\frac{\beta^2}{1+\beta^2} \quad (13)$$

$$\tau_f = \tau_{cr}\,.RV \quad (14)$$

$$\beta = \frac{\gamma_{cr}}{\varepsilon_t} \quad (15)$$

Where γ_{cr} is the concrete shear strain along the crack, τ_f is the shear stress after cracking, τ_{cr} is the shear stress at cracking point , ε_t is the tensile strain, G_c is the concrete shear modulus and β is the ratio between the concrete shear strain along the crack and the tensile strain.

3.2 Steel Reinforcement Model

For reinforcement springs, the model presented by using the bilinear stress-strain relationship developed by [16] as shown in Figure (8). The reinforcement tangent stiffness is calculated depended on the strain from the reinforcement spring and loading status. After reaching the controlled tensile strain (ε_u), the reinforcement bar is assumed to be cut. The force transmitted by the reinforcement bar is redistributed when reaching the failure criterion. Then the residual forces are redistributed to the corresponding prisms in the opposite direction. For cracking criteria, principal stress-based failure criteria is adopted. Figure (8) represents the relation between stress and strain for reinforcement springs under axial stresses. The relation between stress and strain is linear till the yield strain ε_y and the stiffness is linear till yield is regarded as initial stiffness. After yielding, the stiffness is regarded as post-yield stiffness with 10% of the initial stiffness (E_h = 0.1 E_s). The stress-strain relationship is expressed by two straight lines as shown in Equations 16 and 17:

$$f = \varepsilon_S \cdot E_S \qquad \varepsilon_S < \varepsilon_y \qquad (16)$$

$$f = f_y \qquad \varepsilon_S = \varepsilon_y \qquad (17)$$

$$f = f_y + E_h\ (\varepsilon_S - \varepsilon_y) \qquad \varepsilon_S > \varepsilon_y \qquad (18)$$

Where: E_s is the Young's modulus, E_h is the post- yield elastic modulus, ε_s is the reinforcing steel strain crossponding to stress f_s , ε_y is the yield strain and f_y is the yield strength.

Figure (9) represents the relation between stress and strain for reinforcement springs under shear stresses [17] which is linear till failure. The stress-strain relationship is expressed as follows:

$$\tau_s = G_S.\gamma_S \qquad (19)$$

Where G_S is the reinforcing shear modulus, γ_s is the shear strain and τs is the shear stress.

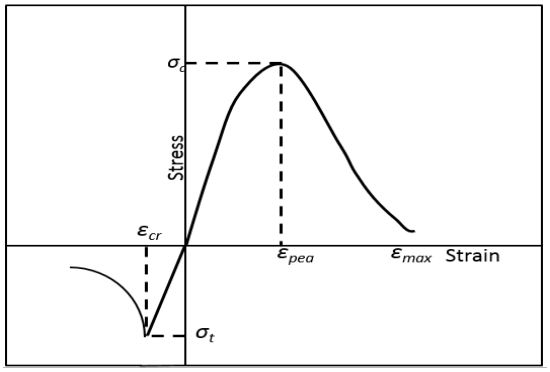

Figure (6) Compression and Tension Models for Concrete [14].

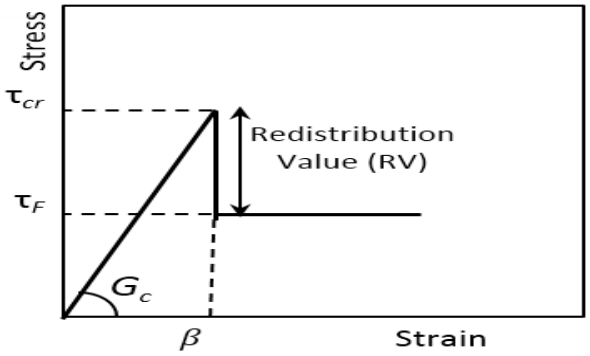

Figure (7) Shear Model for Concrete [15].

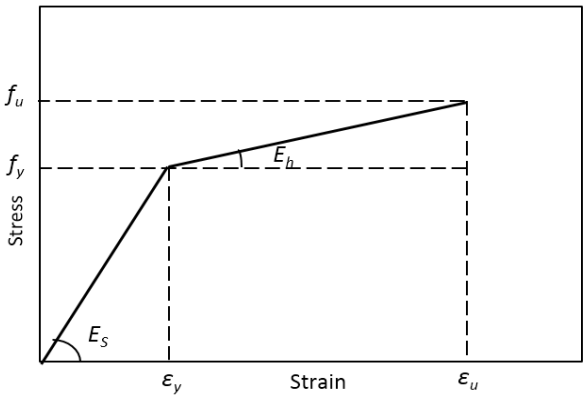

Figure (8) Axial Stress Curve for reinforcing Steel Model [16].

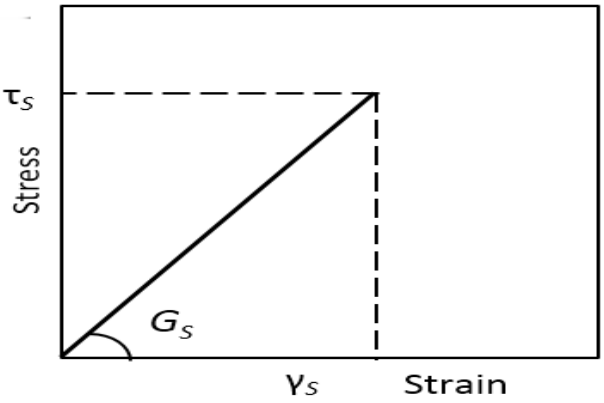

Figure (9) Shear Model for reinforcing Steel [17].

4 VALIDATION of AEM for 2-D FRAMES

4.1 Three-Story R.C Frame

4.1.1 Description of the Numerical Model and the Loading Process

Yi et al. [18] carried out an experimental study for R.C frame to investigate progressive failure due to the loss of a middle central first story column. Figure (10) shows the frame dimensions, height and position of the removal column. The columns and the beams cross sections were modeled as rectangle cross sections as shown in Figure (11-a). Regarding to reinforcement, bottom reinforcement bars were continued through the span and extended to a distance 95 mm after columns faces and top reinforcement was continued through the span and extended above columns as shown in Figure (11-

b). A constant load of 109 kN was applied before progressive collapse testing, to simulate the gravity load of the upper frame. The removed column was modeled as real column and removed after loading beginning process.

Loading process could be summarized through three steps as follow:

1- The self-weight of the structural components is applied then a vertical load of 109 kN is applied incrementally on the top of the middle column;
2- The middle lower central column is removed from model to simulate progressive collapse process;
3- A vertical static displacement at the top of the failed column is increased gradually to simulate the column failure. The loading increment is thus defined as 1.0 mm per step for all models (460 steps were used).

4.1.2 Predicted Behavior and Crack Pattern

Cracks started to appear in the frame at the end of the beam that near the middle column corresponding to vertical displacement of 4 mm. These cracks start to increase and get wider with the increase in the vertical displacement. At latest stage of loading, the cracks were formed near and away from the removed column in the numerical and experimental models as shown in Figures (12) and (13). Due to top and bottom reinforcement continuity, cracks were formed only at the start and at the end of the beams above the removed column.

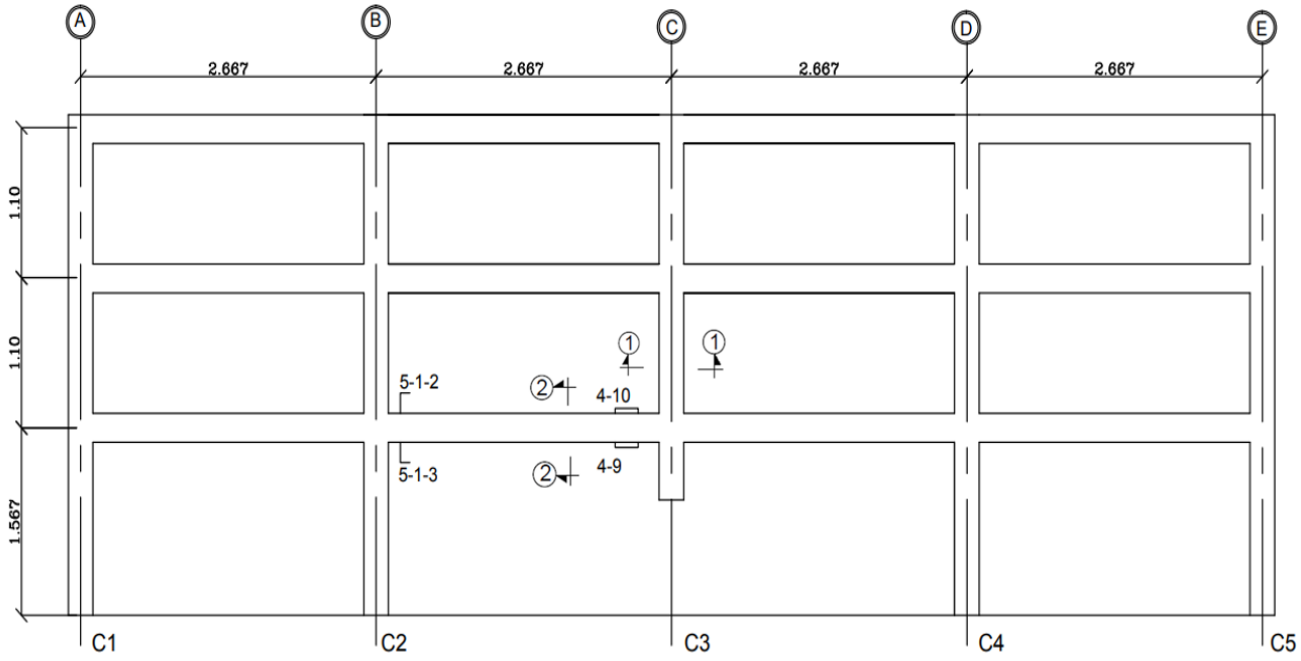

Figure (10) Experimental Tested Frame by Yi et al. [18] (All Dimensions are in mm).

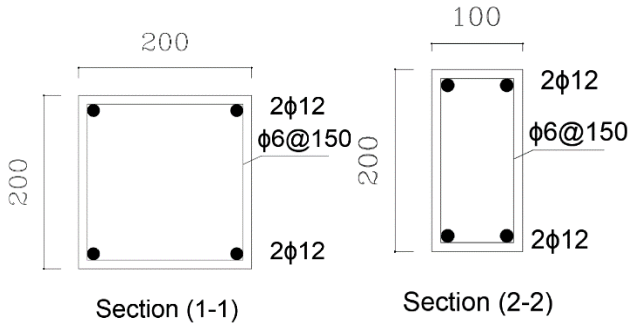

(a) Cross sections for columns and beams (All Dimensions are in mm)

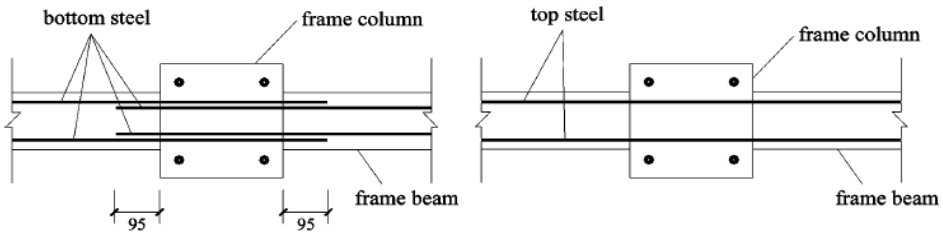

(b) Plan of the top and the bottom beams reinforcement bars extensions

Figure (11) Concrete Dimensions and Reinforcement Details of the Tested Frame [18].

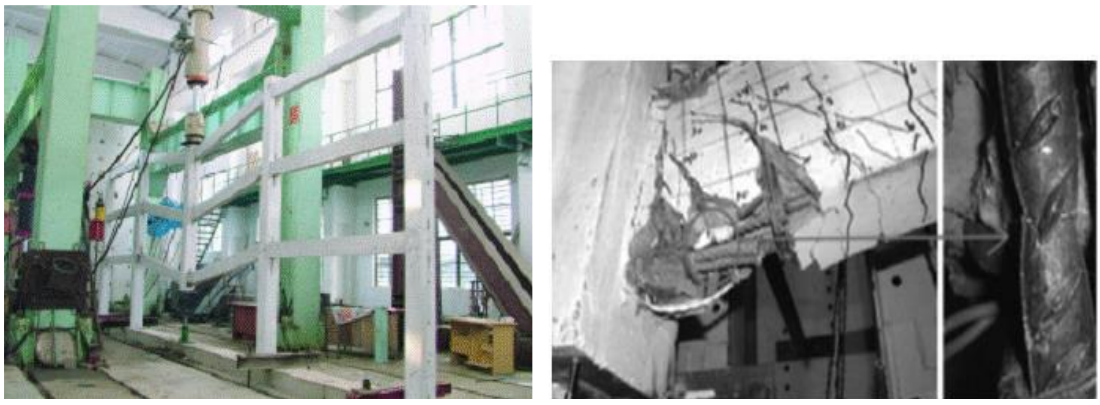

Figure (12) Experimental Crack Pattern [18].

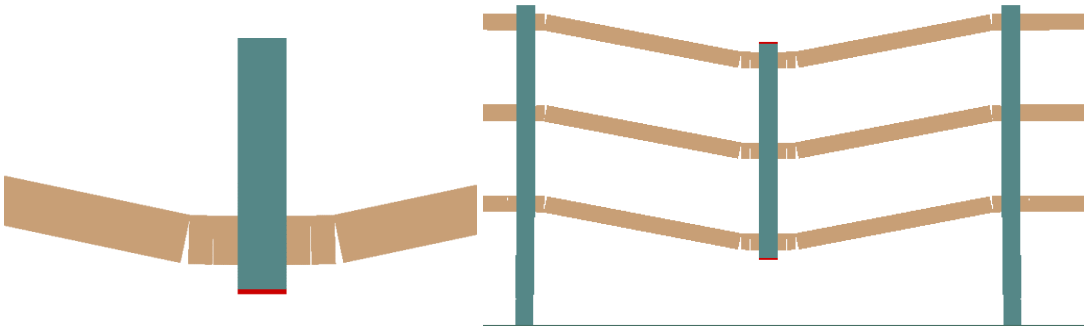

Figure (13) Numerical Crack Pattern [by ELS Software].

4.1.3 Predicted Load-Displacement and Steel-Strain Curves

Figures (14) and (15) show the resisting force versus the applied displacement, top and bottom steel strains respectively, obtained numerical by (ELS software) as well as experimentally. The steel strains were measured and calculated at points (5-1-2) and (5-1-3) as shown in Figure (10). The load transfer mechanisms of the frame against progressive collapse can be divided into four stages.

First stage as shown in part (OA) which can be considered as the elastic stage with cracking of beams observed at this stage and it is represented by the linear relation between the load and the displacement. The displacement of the middle column is less than 25 mm. At elastic stage, the steel strain at point 5-1-2 is in tension and strain value was less than yield strain of steel rebars.

Second stage as shown in part (AB) which can be considered as elasto-plastic stage. At this stage, the ultimate point on the load displacement curve is achieved. The strain of the top steel rebars is tension and the strain at point 5-1-3 is increased in compression.

The third stage as shown in part (BC) is the plastic hinges formation stage. At this stage, the vertical displacement is increased with the reduction of resisting force. The reduction of progressive collapse potential is due to losing of flexural beams capacities due to cracks formed in the compression zone in beams. At this stage, strain at 5-1-2 starts to increase rapidly in tension. However, strain at point 5-1-3 begins to transfer from compression toward tension strain.

The fourth stage as shown in part (CD), the resistance of frame is increased again due to the catenary action mechanism. At this stage, the load of the removed column transfers due to tension force formed in beams after spreading of cracks from compression zone to tension zone and losing of flexural beams capacity. This explains the rapid increase in strain at 5-1-2 and transforming of steel strain at 5-1-3 from compression to tension.

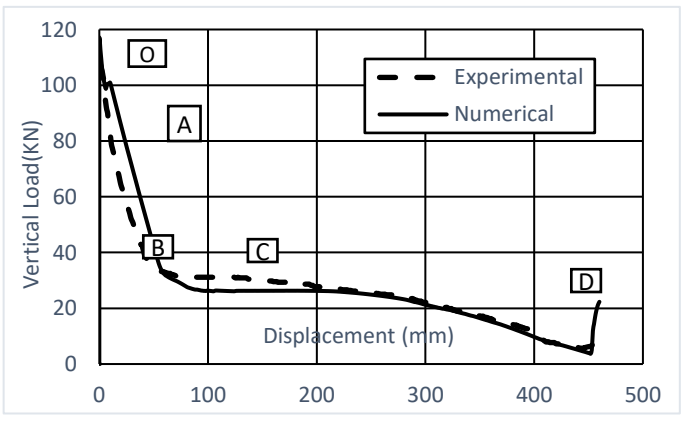

Figure (14) Experimental vs. Numerical Load-Displacement Curve.

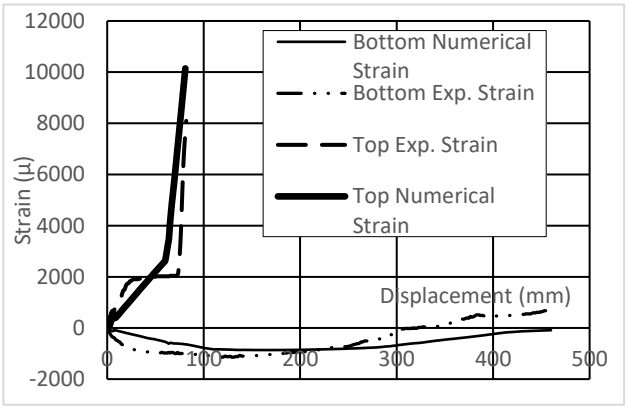

Figure (15) Experimental vs. Numerical Steel Strain Curve.

4.2 Two-Story R.C Frame

4.2.1 Description of the Numerical Model and the Loading Process

Stinger [19] carried out a static experimental study for a two-story R.C frame structure to better understand the collapse resistance mechanisms of reinforced concrete frames. The frame consists of two bays with equal spacing 1.83 m between columns center to center and height of each story was 0.91 m. Bottom, top bars extensions and stirrups arrangements are shown in Figure (16). Rectangle sections were modeled with the same concrete dimensions and reinforcement details used in experimental test as shown in Figure (17). The numerical simulation of the gradual failure of the first-story middle column is performed in a displacement-controlled manner as follows: the self-weight of the structural components applied first then; a vertical static displacement of this node is increased gradually to simulate the column failure. The loading increment is thus defined as 0.75 mm per step for all models 500 steps were used. The short cantilevers were allowed to rotate and move vertical and prevented from horizontal displacement during the simulation as performed in experimental test.

4.2.2 Predicted Behavior and Crack Pattern

Upon loading, the frame initially responded in an elastic state and at displacement of 30 mm cracks start to appear at locations where the negative moment reinforcement bars stopped (non- continuous reinforcement bars), which ended at 300 mm from the face of the outer columns. These cracks form in all four beams. As load increased, the cracks extended, widened and plastic hinges start to form at the same locations of cracks starting. In addition to these cracks, plastic hinges formed also near to the center column. The predicted pattern is in a good agreement with the observed pattern as shown in Figures (18) and (19).

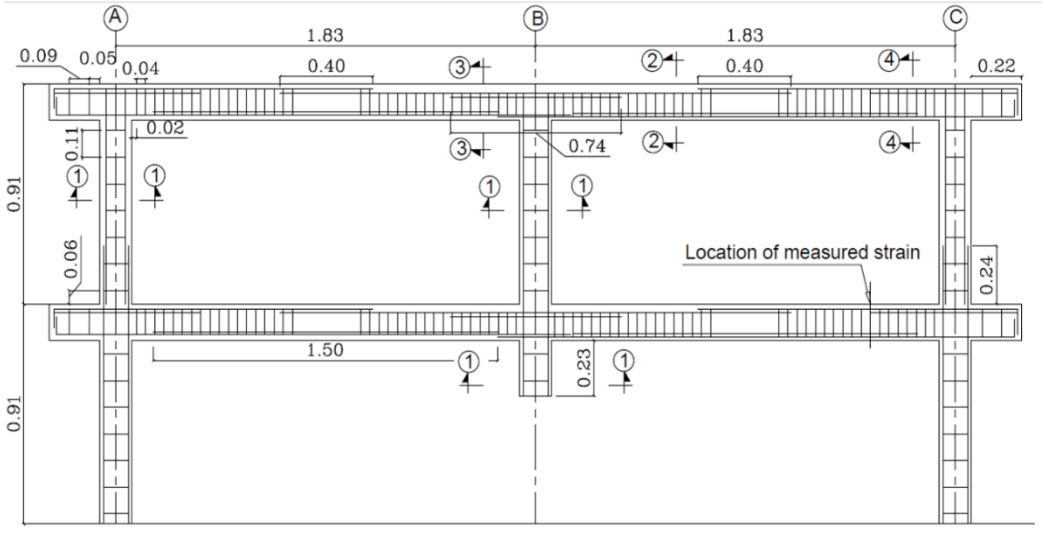

Figure (16) Concrete Dimensions and Reinforcement Details of 2-D 2-Story Frame [19] (All Dimensions are in mm).

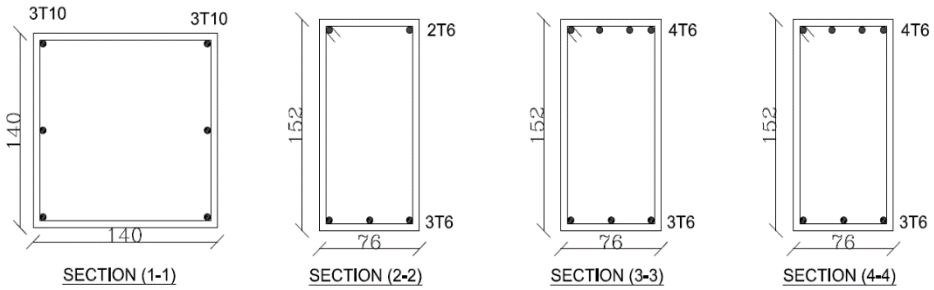

Figure (17) Cross Sections of Columns and Beams of the 2-D , 2-Story Frame [19] (All Dimensions are in mm).

Figure (18) Observed Crack Pattern for the Experimental Tested Specimen (2-D 2-Story Frame) [19].

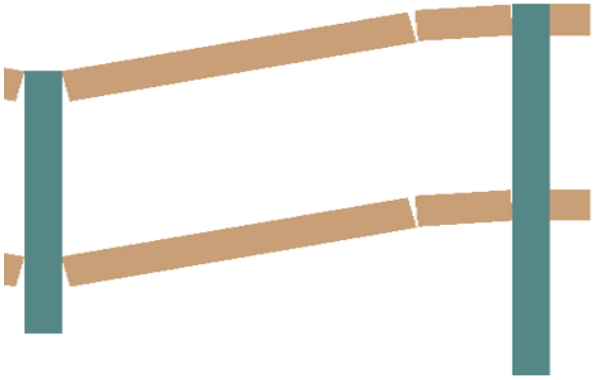

Figure (19) Numerical Crack Pattern (2-D 2-Story Frame) [by ELS Software].

4.2.3 Predicted Load and Steel Strain Curves

Figure (20) shows the relation between the resisting force and the applied displacement at the top of the removed middle column representing by section (1-1) in Figure (17). Figure (21) shows the steel strains measured during experimental test and the top and the bottom steel strain calculated numerically. The location of the measured points is indicated in Figure (16). The simulation of the middle removable column along with the increase in the vertical displacement may be divided into four stages.

Part (OA) represent the first stage on the curve and can be considered as the elastic stage. A linear relation between the resisting force and displacement is observed, representing the flexural action of the frame. The measured strain at the bottom point equals to 0.0001 in compression which near to the corresponding strain on the predicted curve as shown in Figure (21). The experimental value of strain at the top of the beam was in tension.

Elasto-plastic stage can be observed in the second stage on the curve in part (AB). At this stage, the displacement was measured 68 mm and the frame reach to ultimate state. The strain in the steel bars exceed the yield limit and the resistance of the frame is still increasing with displacement due to the compression value of steel strain at bottom which indicates that the beam subjected to compression force as shown in Figure (21). The generated compression force leads to improve the flexural capacity of the frame. This stage represents the arch compression action of frame.

Part (BC) represents the plastic hinges formation stage, where the displacement of the middle column was increased to 150 mm. The resisting force of the frame was decreased due to losing flexural capacity of the frame. This stage represents also the compression action of the frame but the bottom steel strain curve at this stage is started to convert form compression to tension at point 220 mm and the top steel strain curve was increased sharply after the same point as appeared in Figure (21).

In part (CD) (stage four), the resistance of the frame is due to catenary action mechanism at which the resistance increases gradually again till failure. This mechanism depends on the tension forces generated in the beams. At this stage the bottom and the top strains are in tension as presented in Figure (21).

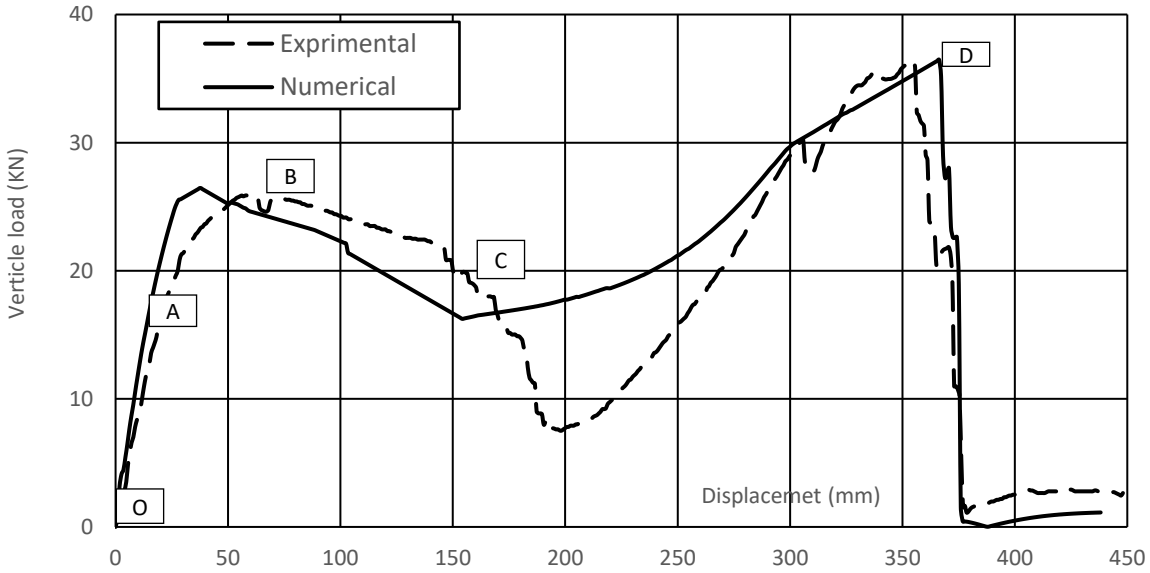

Figure (20) Experimental vs. Numerical Load-Displacement Curve.

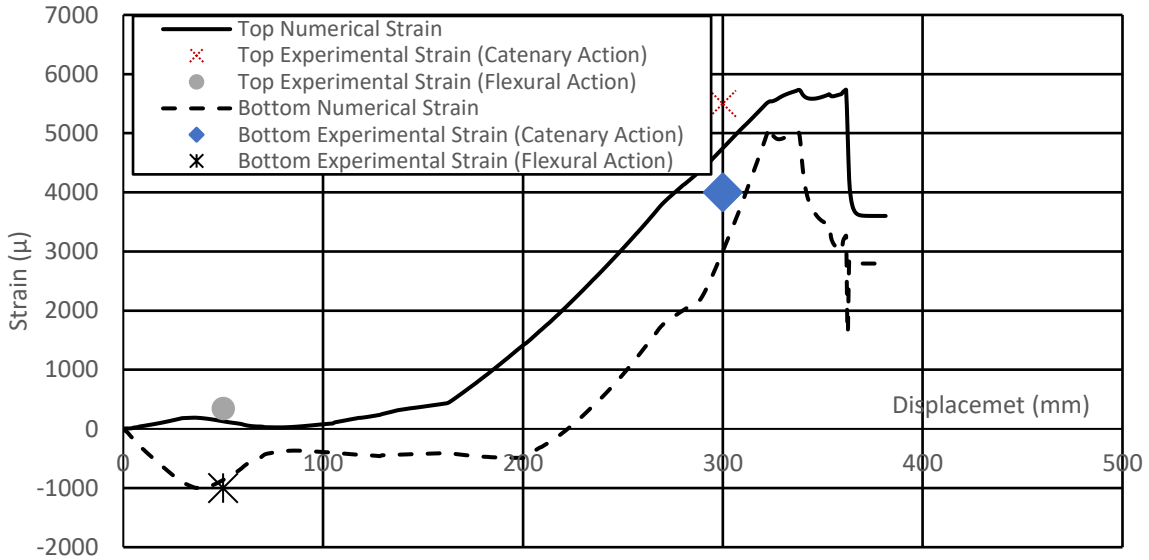

Figure (21) Predicted and Measured Strains of the Bottom and the Top Steel Bars.

5 Validation of AEM for 3-D Frames

5.1 3-D Single-Story R.C Frame – Corner Column Removal Study

5.1.1 Description of the Numerical Model and the Loading Process

In Ref. [20] a single story with four bays was established. The overall dimensions of the tested frame were 3.6 m x 2.6 m in plan and the height was 1.75 m as shown in Figure (22). Column sectional dimension were 133 mm x 133 mm. The beams in the longitudinal direction were 67 mm x 150 mm, while the transverse beam dimensions were 67mm x 117mm and the floor thickness was 30 mm as shown in Figure (23). Bottom reinforcement of the slabs was a mesh T3-30 mm in the whole spans and the top reinforcement was T3-30 mm above all beams – column connections only as shown in Figure (22). The removed corner column was at intersection between axis (A) and axis (3). The numerical simulation of the gradual failure of the corner-column is performed in a displacement-controlled manner as follows; the self-weight of the structural components applied first then, a vertical static displacement at the removal column is increased gradually to simulate the column failure. The loading increment is thus defined as 0.3 mm per step where 500 steps were used.

5.1.2 Predicted Behavior and Crack Pattern

When the vertical displacement at the removed corner column position was only 3 mm at the first stage of loading, cracks begun to form at end of beam (C) away from the removed column. When the vertical displacement was 7 mm, cracks started to form at end of beam (B) away from the removed column as shown in Figure (24). As the displacement increased, beams (B) and (C) gradually twisted inward, due to shear cracks at the beams ends. The predicted and the experimental crack patterns show good agreement. At the same time, the slab panel (P1) had several cracks started to propagate from the first stage of loading. Increasing loading leads to increase the diagonal cracks to be widen and large as shown in Figure (25). A small number of cracks appeared at the middle of the (P2) and (P4) slabs that surrounding the fallen bay.

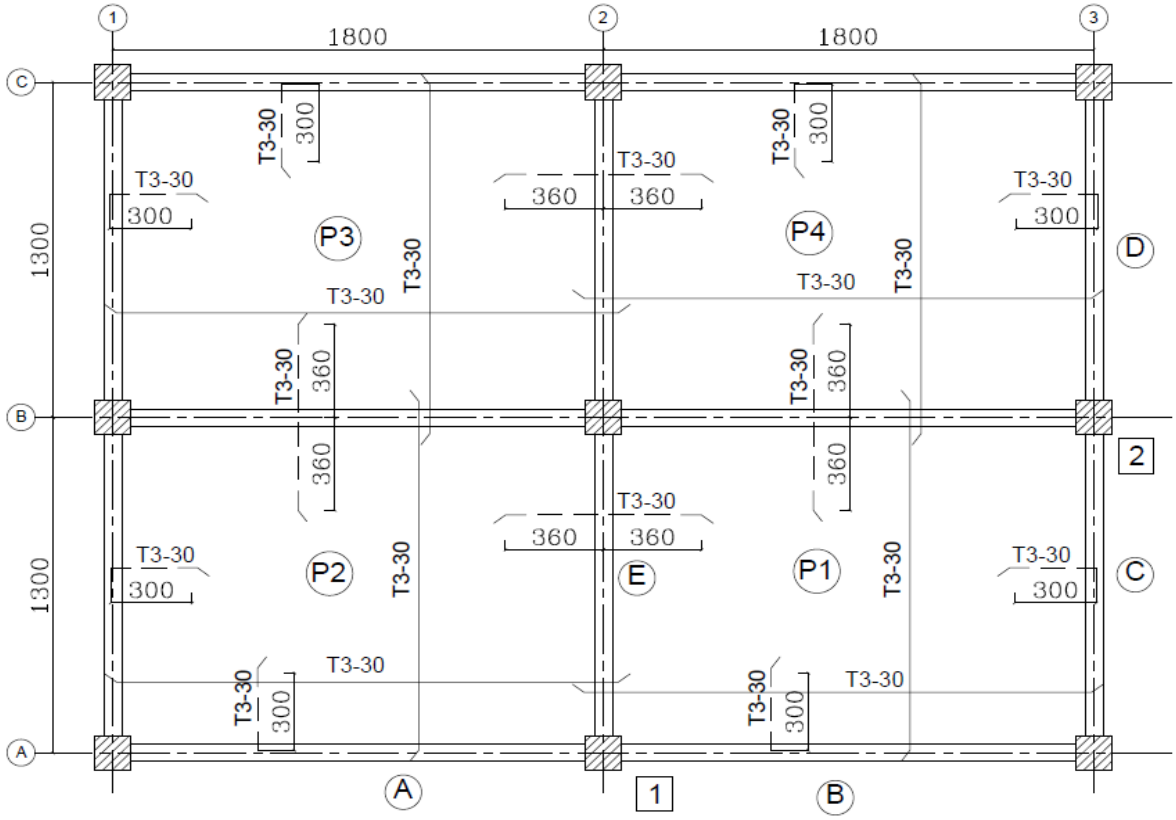

Figure (22) Layout of the Slab and its Reinforcement Arrangement for the 3-D Single-Story Frame [20] (All Dimensions are in mm).

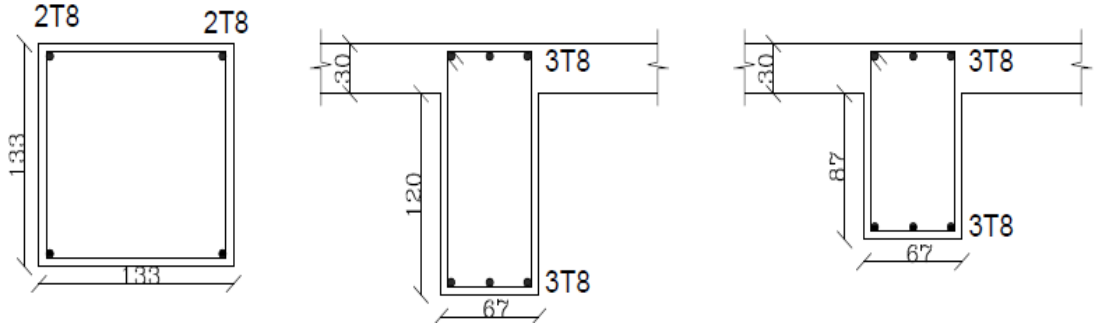

(a) Column Cross Section (b) Longitudinal Dir. Beam Cross Section (c) Transverse Dir. Beam Cross Section

Figure (23) Beams and Columns Cross-Sections for the 3-D Single-Story Frame [20]. (All Dimensions are in mm)

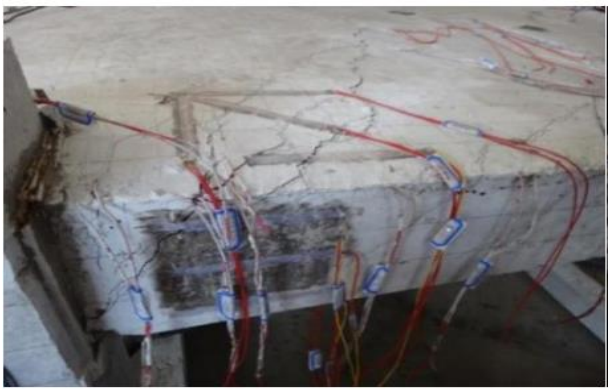

(a) Experimental Cracks of Beam (B) [20]

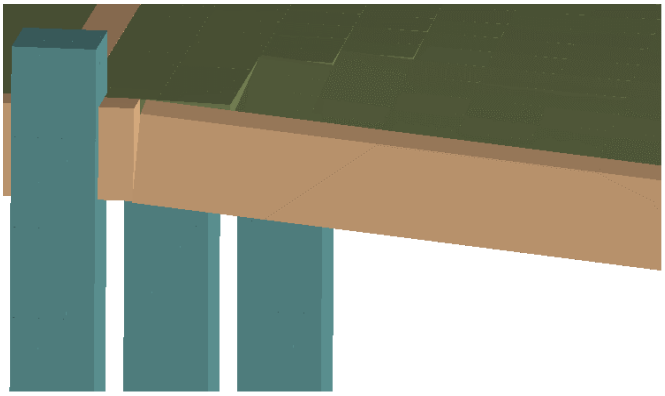

(b) Numerical Cracks Pattern of Beam (B) [by ELS Software]

Figure (24) Experimental and Numerical Cracks of Beam (B) for the 3-D Single-Story Frame [20].

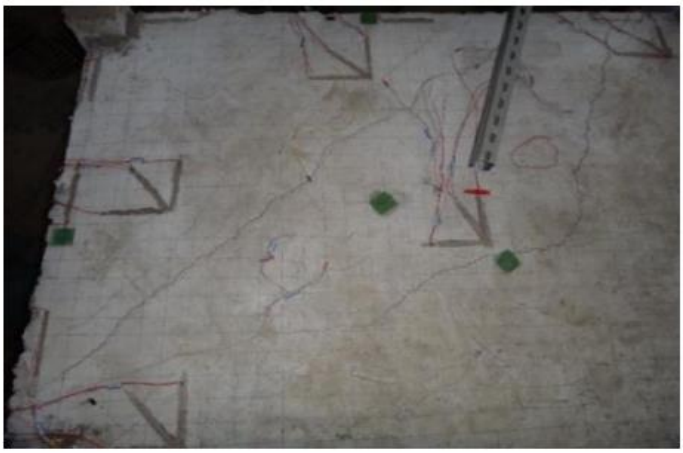

(a) Experimental Cracks of Slab (P1) [20]

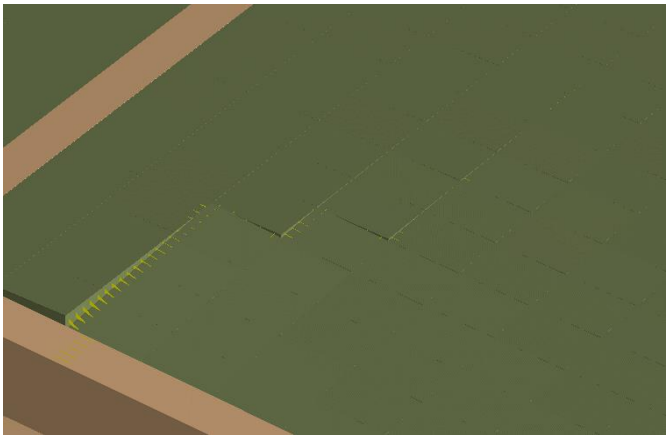

(b) Numerical Cracks Pattern of Slab (P1) [by ELS Software]

Figure (25) Experimental and Numerical Cracks of the Slab (P1).

5.1.3 Predicted Load Displacement and Steel Strain Curves

Figure (26) shows the numerical and the experimental resisting force versus the applied displacement at the top of the removed corner column representing by columns cross section in Figure (23). Figures (27) and (28) show the measured and the predicted top and bottom strains at points (1) and (2) of the longitudinal and transverse beam at location away from the removed column. The behavior can be simulated throughout four stages as follow:

First stage, (part (OA)), can be considered as the elastic stage with cracking of beams. The displacement of removed column was less than 4 mm. linear relation between the resisting load and the loading displacement can be observed.

Second stage (part (AB)), can be considered as the elasto-plastic stage. At this stage, strain of the steel bars subjected to tension has excessed the yield limit and frame reaches the ultimate state. Reduction of the resisting load can be observed at part (BC). This stage can be considered as the plastic hinges formation stage at which displacement of the fallen column was increased to 44 mm and the resistance of the frame after ultimate is decreased due to cracks propagation in beams, but not fallen, due to existence of slabs.

In part (CD), the resistance of the frame still constant at level of 12.5 kN although loading displacement increased due to existence of the slab that form another mechanism for load transfer with the catenary action formed in the beams. Slabs contribute with membrane action that increase the potential of the frame against progressive collapse in the final stage. Catenary action for beams and tensile membrane action for slabs generated when the beam axial force changed from compression to tension since the nature of catenary action is a tensile mechanism. Numerical and experimental force deformation curves show a generally similar pattern.

Figure (27) shows the relationship between top and the bottom steel bars stains and the vertical displacement at the removed corner column at the far end of beam (B) at position 1 as shown in Figure (22). Top bars strain was in tension. The strain increased slightly to reach 0.00022, indicating the elastic behavior. Then, strain started to increase sharply after this point which indicates plastic mechanism formation. Then, the strain was contained in sharply increase due to catenary action mechanism. The strain at the bottom bars, was compression. Strain decreased slightly to reach the maximum strain value due to compression zone of the cantilever bending moment.

Similar to beam (B), strains at the far end of beam (C) at position 2 was investigated as shown in Figure (22). Top bars strain increased slightly to reach 0.00025 in a linear relation indicating elastic behavior. Then, a sharply increased in strain after this point that indicates plastic hinge formation. The strain was continued increasing sharply indicting catenary action. Bottom bars strain decreased slightly

to reach the maximum strain value 0.0003. The strain is continued in compression and decreased slightly till failure point.

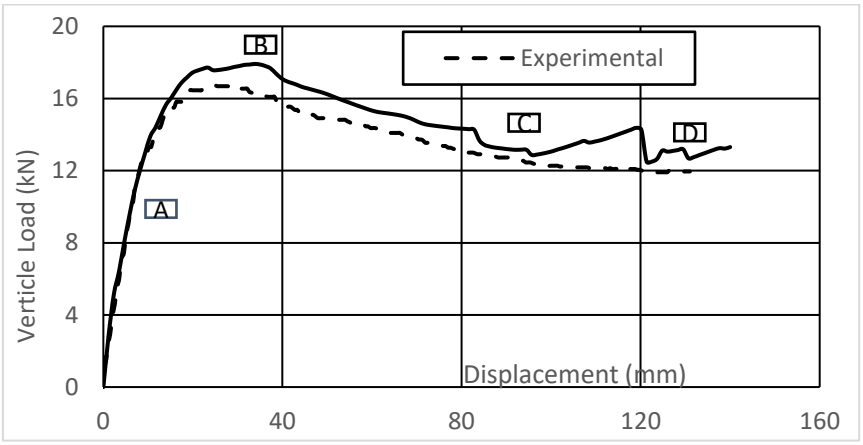

Figure (26) Experimental vs. Numerical Load-Displacement for 3-D Single-Story Frame [20].

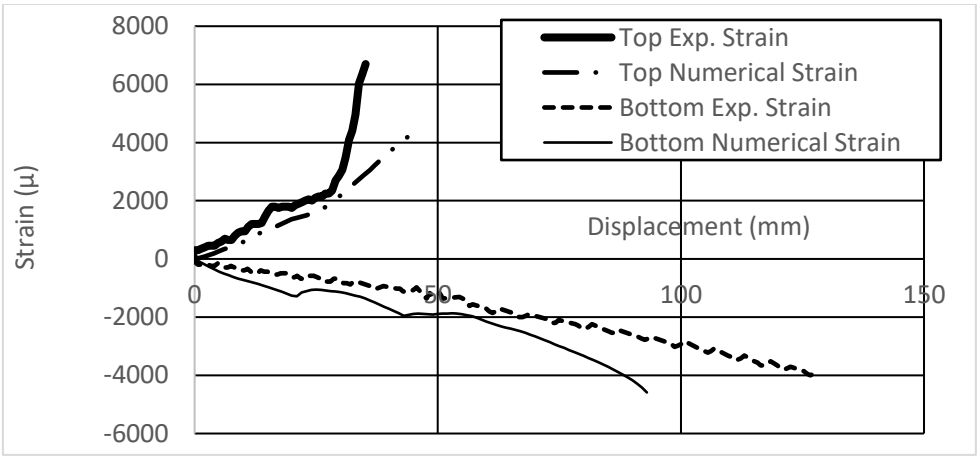

Figure (27) Experimental vs. Numerical Steel Strain Curve at Position (1) for the 3-D Single-Story Frame [20].

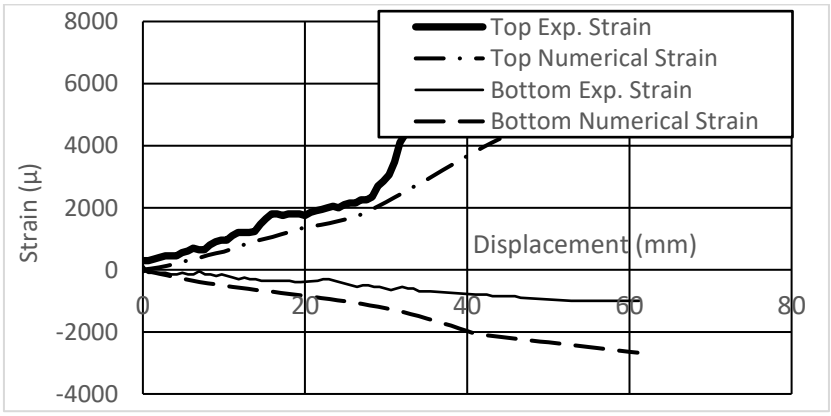

Figure (28) Experimental vs. Numerical Steel Strain Curve at Position (2) for the 3-D Single-Story Frame [20].

5.2 Single Story R.C Frame– Edge Column Removal Study

5.2.1 Description of the Numerical Model and the Loading Process

In Ref. [21] a single story with four bays was tested in order to study the contribution of the slabs on progressive collapse mechanism. The overall dimensions of the tested frame were 3.6 m x 2.6 m in plan and 1.2 m height as shown in Figure (29). Column cross sectional dimensions were 135 mm x 135 mm, beams at axes A, B and C have cross-sectional dimensions 70 mm x 150 mm. Beams at axes 1, 2 and 3 cross-sectional dimensions were 70 mm x 120 mm and floor thickness was 30 mm as shown in Figure (30). Bottom reinforcement of slab was a mesh T3-30 mm in the whole spans and top reinforcement was T3-30 mm above all beams only as shown in Figure (29). The removed edge column was at intersection between axis (A) and axis (2). The numerical simulation of the gradual failure of the central-column is performed in a displacement-controlled manner as follows: the self-weight of the structural components applied first. Then, a vertical static displacement of this node is increased gradually to simulate the column failure. The loading increment is thus defined as 0.7 mm per step for all models (500 steps were used). The two bays adjusted to the removed column were divided into small meshing of elements more than the other bays.

5.2.2 Predicted Behavior and Crack Pattern

Upon loading, the frame passes through several stages during failure process. At the first stage of loading, when the vertical displacement of the edge removed column was less than 5 mm under the action of the self-weight, cracks started to form in longitudinal beam end that located away from the removed column as shown in Figure (31), then cracks formed in beam in the transverse direction at same end. When the vertical displacement was 29 mm, cracks start to appear at the slabs especially in the zone adjusted to the removed column as shown in Figure (32), while for the part of slab away from the removed column, cracks were so small in compared to the other zone related to the removed column. As the displacement continued to increase, reached to 68 mm, cracks in slabs and beams spread in large scale. Up to displacement 100 mm, cracks noticed in the compression zone in the longitudinal beams and in the slabs, while beam in the transverse direction subjected to partial failure due to lack of lateral supports or constrains, where it works as cantilever after the fallen of column.

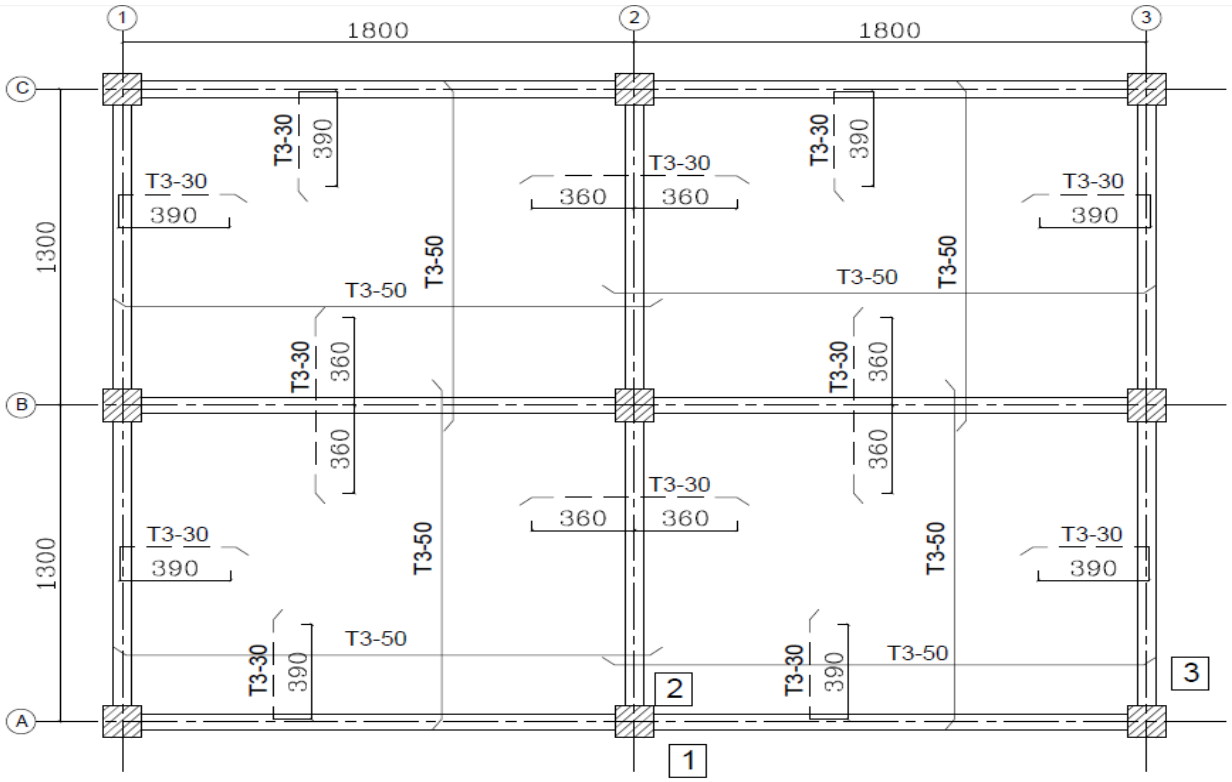

Figure (29) Layout of the Slabs and its Reinforcement Arrangement for the 3-D Single-Story Frame [21] (All Dimensions are in mm).

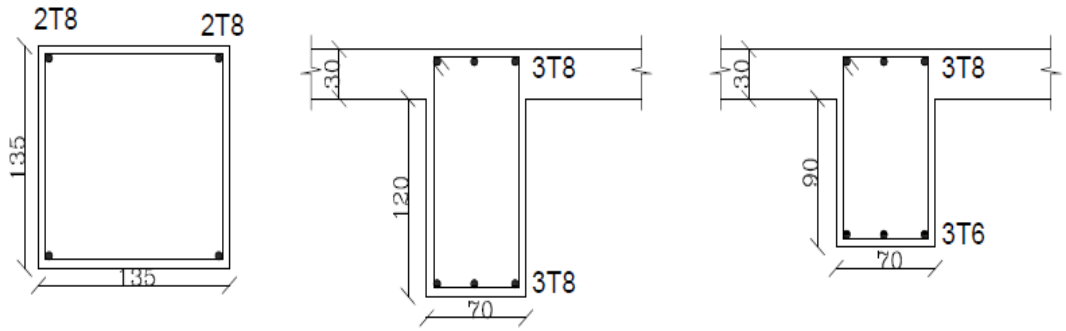

(a) Column Cross Section

(b) Longitudinal Dir. Beams Cross Section

(c) Transfers Dir. Beams Cross Section

Figure (30) Beams and Columns Cross-Sections for the 3-D Single-Story Frame [21] (All Dimensions are in mm).

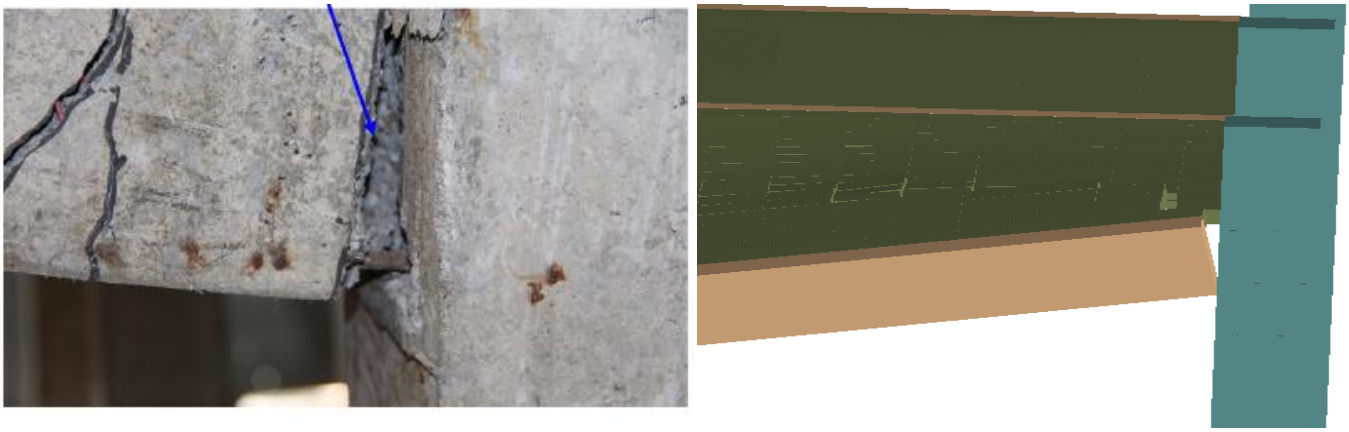

(a) Experimental Cracks at the Longitudinal Beam [21]

(b) Numerical Cracks Pattern at the Longitudinal Beam [by ELS Software]

Figure (31) Experimental and Numerical Cracks at the Longitudinal Beam for the 3-D Single-Story Frame [21].

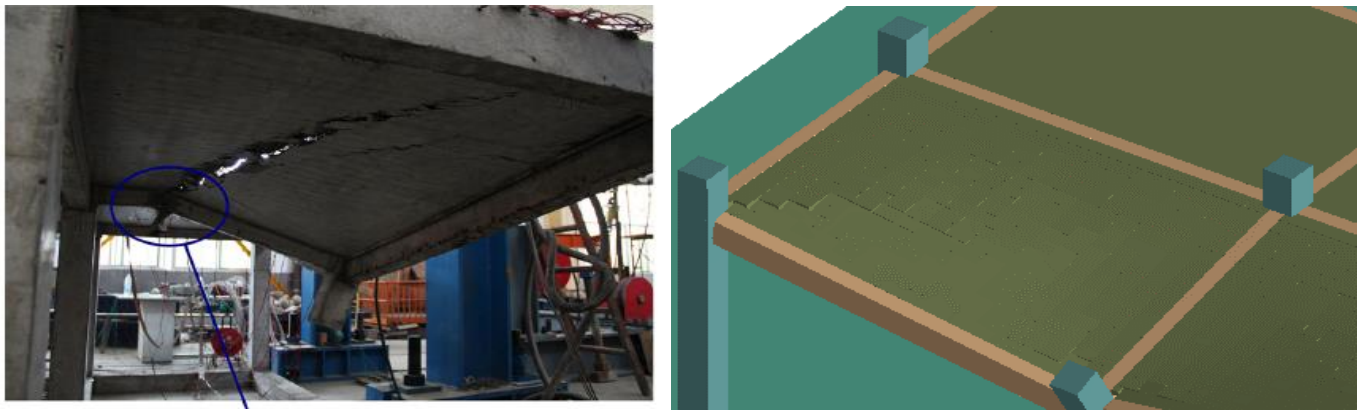

(a) Experimental Cracks for Slabs [21]

(b) Numerical Cracks Pattern for Slabs [by ELS Software]

Figure (32) Experimental and Numerical Cracks at Slabs for the 3-D Single-Story Frame [21].

5.2.3 Predicted Load Displacement and Steel Stress Curves

Figure (33) shows the resisting force versus the applied displacement at the top of the removed central edge column obtained numerically by (ELS) as well as experimentally. It can be noticed that, the simulated failure of the column along with the increase in the vertical displacement may be divided into four stages.

In the first stage, (part (OA)) which can be considered as the elastic stage with cracking of beams predicted at this section. This stage represents the linear relation between the load and displacement and define the flexural resistance of the frame.

Second stage, (part (AB)) which can be considered as the elasto-plastic stage at which the frame reaches to the ultimate state and the strain in steel bars exceed the yield limit. This stage represents the start of arch compression action mechanism through load transfer mechanism.

Part (BC) represents the plastic hinges formation stage, at this stage displacement of fallen column was increased to 105 mm and strain of steel bars at this displacement has excessed the yield limit and expresses the continuity of compression arch action mechanism. The increasing rate of the vertical load in this stage with increasing vertical displacement of the removed column decreased significantly, and the deformations were dominated by plastic rotations of the beams.

In part (CD), the load starts to increase again throughout another load transfer mechanism. These mechanisms represent the composite mechanisms between the catenary action of the longitudinal beam and the tensile membrane mechanism of the slabs. For the tensile membrane mechanism, the internal area of the slabs away from the fallen column are surrounded by the negative moment, and the areas of progressive collapse adjusted to fallen column were surrounded by positive moment. This mechanism increases resistance of the frame as shown in Figure (33). The resistance of the frame increased till displacement 350 mm and still increasing due to tensile membrane mechanism of slabs.

Figure (34) shows the relationship between the top and the bottom steel bars stress and the vertical displacement of experimental results and the numerical ones. Stresses were predicted at the near end on the longitudinal beam at position (1) as shown in Figure (29). Throughout the first and second stage of loading mentioned before, stress at top steel was in compression till displacement 75 mm which represent the end of elasto-plastic stage. Then the top reinforcement changed to tension in the plastic hinge formation stage and the tensile stress increased with displacement increase. The increase in the tensile stress was due to subjecting of beams to tension forces coming from the mix between catenary action of beams and membrane action of slabs. Bottom reinforcement was in tension and the stress was almost linearly increased with increasing in the vertical displacement of the removed column.

Then the bottom reinforcement entered the yield state at displacement 70 mm, after that it had entered the strain-hardening range till displacement 350 mm.

Figure (35) shows the relationship between the top and the bottom steel bars stress and the vertical displacement of the fallen edge column for both experimental and numerical results. Stresses were predicted at the near end on the transverse beam at position (2) as shown in Figure (29). Top reinforcement was in compression and the value has compression during all loading process, due to lack of lateral support. Bottom reinforcement was in tension, then it entered the yield state at displacement of 30 mm, after that stress increased gradually till failure.

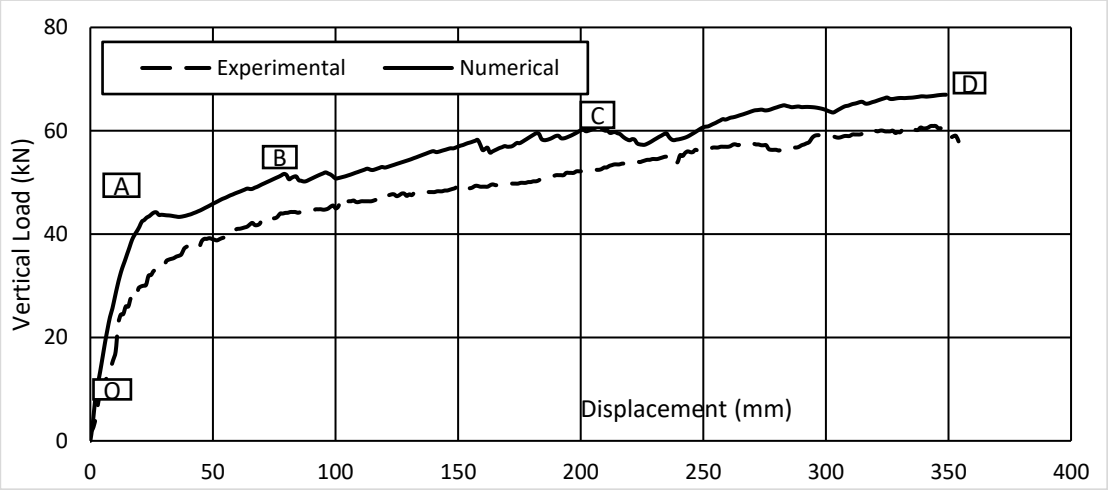

Figure (33) Experimental vs. Numerical Load-Displacement Curve for the 3-D Single-Story Frame [21].

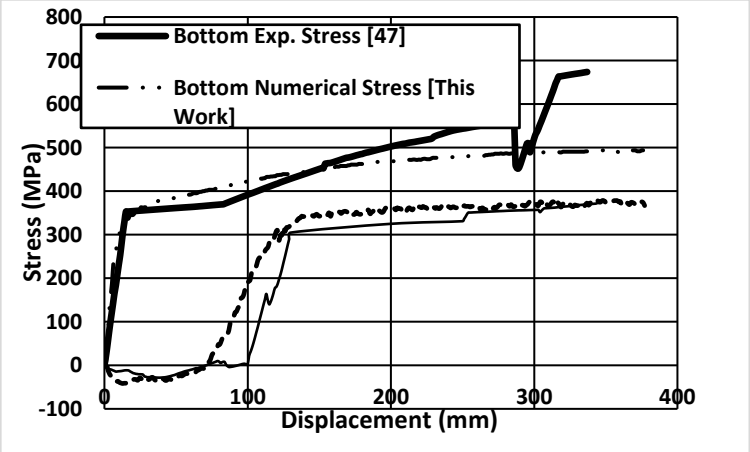

Figure (34) Experimental vs. Numerical Steel - Stress at Position (1) for the 3-D Single-Story Frame [21].

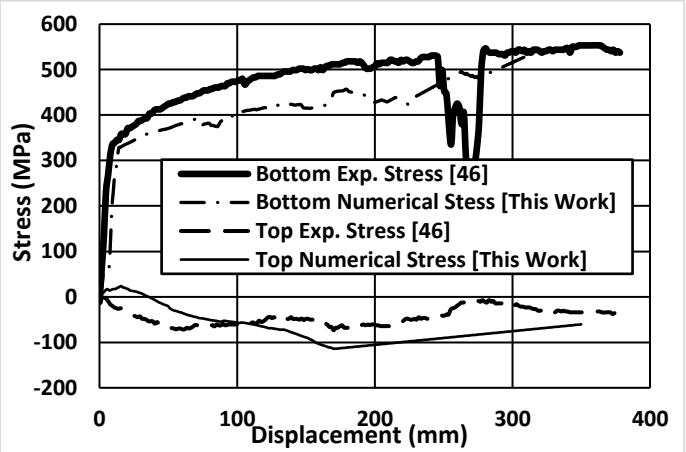

Figure (35) Experimental vs. Numerical Steel Stress at Position (2) for the 3-D Single-Story Frame [21].

6 CONCLUSION

The following points are drawn from the research:

1- (ELS) software is demonstrated its superior ability to represent the post- ultimate stages, including the plastic hinge formation and catenary action stages. For the studied R.C frames, the obtained numerical results of the load-deformation curves, concrete and steel strains are well matched with experimental ones for both 2-D and 3-D R.C frames.

2- The ability of (ELS) is verified to simulate the R.C frames with different slabs arrangement in the space. Predicted crack patterns obtained from the numerical models in all the studied frames are matched with the cracks formed experimentally.

3- For the 2-D R.C frames, after column removal event, the reinforced concrete frame is subjected to partial failure and passed through different stages till the total failure. The first stage is the elastic stage; the frame transfers the load of the removed column by shear forces due to flexural beam capacity. Then the frame transfers to another stage after the reinforcing steel yielding, called elasto-plastic stage. The third stage called plastic hinge formation stage. At this stage, frame loss the flexural capacity and cracks are spread in the compression section zone. The last stage is the catenary stage, at this stage the removed column transfer is due to tension force formed in beams and this mechanism develops after applying large deformation in (ELS).

4- For the 3-D R.C frames, the mechanisms to resist progressive collapse are the same of the mechanisms of the 2-D R.C frames except the last mechanism of resistance called catenary action. Slabs contribute throughout the last mechanism with membrane action mechanism that begin after plastic hinge formed in beams and losing of flexural capacity process.

REFRENCES

[1] Applied Science International, “Extreme Loading for Structures”, Theoretical Manual, Durham, NC, (2013).

[2] Pearson, C., and Delatte, N., “Lessons from the Progressive Collapse of the Ronan Point Apartment Tower”, Proceedings of the 3rd ASCE Forensics Congress, October 19 - 21, (2003), San Diego, CA.

[3] Corley, W. G., Mlakar, P. F., Sozen, M. A., and Thornton, C. H., “The Oklahoma City Bombing: Summary and Recommendations for Multi-hazard Mitigation,” Journal of Performance of Constructed Facilities, (1998), Vol. 12, No. 3, pp.100–112.

[4] NIST, “NIST’s World Trade Center Investigation”, National Institute of Standards and Technology, (2008), U.S. Department of Commerce.

[5] General Services Administration (GSA), “Alternate Path Analysis and Design Guidelines for Progressive Collapse Resistance”, Washington DC: General Services Administration, (2013).

[6] Department of Defense (DoD), “Unified Facilities Criteria, Design of Buildings to Resist Progressive Collapse”, Washington DC: Department of Defense, (2009).

[7] Yi WJ, Yi F, Zhou Y. Experimental studies on progressive collapse behavior of RC frame structures: advances and future needs. International Journal Concrete Structural Materteral, (2021); 15(1): 1–23.

[8] Zhang XY, Zhao YG, Lu ZH. An efficient method for time-variant reliability including finite element analysis. (Reliab Eng Syst Saf), (2021); 210:107534.

[9] Zhang Qiang, Zhao Yan-Gang, Xu Lei. Upgrading of reinforced concrete frame using novel detailing technique for progressive collapse prevention. (Bull Earthquake Eng), (2022):1–20.

[10] Tagel-Din, H. S. and Meguro, K., “Nonlinear Simulation of R.C Structures Using Applied Element Method”, Structural Engineering Earthquake, JSCE, 17(2), (2000c), pp. 137s-148s.

[11] Meguro, K. and Tagel-Din, H, “Applied Element Method for Structural Analysis: Theory and Application for Linear Materials”, Structural Engineering /Earthquake Engineering., International Journal of the Japan Society of Civil Engineers (JSCE), (2000) 17, 21s-35s.

[12] El-Gamal, A., R., “Reducing Progressive Collapse in Reinforced Concrete Building Structures” Ph.D. Thesis, Benha Faculty of Engineering, Benha University, (2018).

[13] El-Shaer, A., “Progressive Collapse Assessment of Multistory Reinforced Concrete Structures Subjected to Seismic Actions”, M.Sc, Cairo University, (2013).

[14] Okamura, H. and K. Maekawa, “Nonlinear Analysis and Constitutive Models of Reinforced Concrete”, (1991), Gihodo Co. Ltd., Tokyo.

[15] Kupfer,H., Hilsdorf, H.K. and Rusch, H., “Behavior of Concrete under Biaxial Stresses”. ACI Journal, (1969), 66, 656-666.

[16] Ristic, D., Yamada, Y., and Iemura, H., "Stress-Strain Based Modeling of Hysteretic Structures under Earthquake Induced Bending and Varying Axial Loads", (1986), Research Report No. 86-ST-01, School of Civil Engineering, Kyoto University, Kyoto, Japan.

[17] Al-Hafian, S., "Seismic Progressive Collapse of Reinforced Concrete Frame Structures using the Applied Element Method", Ph. D Thesis, School of the Built Environment of Heriot, Watt University, (2013).

[18] Yi, W. J., He, Q. F., Xiao, Y., and Kunnath, S. K, "Experimental Study on Progressive Collapse-Resistant Behavior of Reinforced Concrete Frame Structures", ACI Structural Journal, (2008), 105(4), 433–439.

[19] Stinger, S., M., "Evaluation and Valuation of Alternative Resistance Mechanisms for Progressive Collapse", M.Sc., Faculty of Graduate School, University of Missouri-Columbia, (2011).

[20] Zhou, Y., Li, F., Wang, S., and Zhao, N., "Experimental Research of Progressive Collapse Resistance of R.C Frame Structure", Journal of the Faculty of Engineering, (2011), Vol. 31, No.7, pp. 152-161.

[21] Hou, J., and Song, L., "Progressive Collapse Resistance of R.C Frames under a Side Column Removal Scenario: The Mechanism Explained", International Journal of Concrete Structures and Materials, (2016), Vol.10, No.2, pp.237–247.